Title

Time domain probabilistic seismic risk analysis using ground motion prediction equations of Fourier amplitude spectra

Authors
Wang, Hexiang
Wang, Fangbo
Yang, Han
et al.

Publication Date
2022-06-01

DOI
10.1016/j.soildyn.2022.107218

Time Domain Probabilistic Seismic Risk Analysis using Ground Motion Prediction Equations of Fourier Amplitude Spectra

Hexiang Wang[a], Fangbo Wang[b], Han Yang[a], Yuan Feng[a], Boris Jeremić[a,c,*]

[a] *Department of Civil and Environmental Engineering, University of California, Davis, CA, USA*
[b] *School of Civil Engineering, Tianjin University, China*
[c] *Earth and Environmental Science Area, Lawrence Berkeley National Laboratory, Berkeley, CA, USA*

Abstract

Modeling of Fourier amplitude spectra (FAS) of seismic motions has gained much attention in engineering seismology. In the past few years, several ground motion prediction equations (GMPEs) and inter-frequency correlation structure of FAS have been established. Due to many preferable characteristics of FAS, probabilistic seismic hazard/risk analysis is rapidly changing from ergodic, spectrum acceleration $Sa(T_0)$-based approach to non-ergodic, site-specific, FAS-based approach. This paper presents time domain intrusive framework for probabilistic seismic risk analysis using GMPE of FAS. Methodology for time domain stochastic ground motion modeling based on GMPEs of FAS is presented in some detail. The simulated uncertain motions are modeled as a random process and represented by polynomial chaos Karhunen-Loève expansion. The random process excitations are further propagated into the uncertain structural system using Galerkin

*Corresponding author
Email address: jeremic@ucdavis.edu (Boris Jeremić)

stochastic finite element method (SFEM). Probabilistic evolution of structural response is solved, and such solution is used to develop seismic risk for any damage state. The presented framework is illustrated through seismic risk analysis of a four-story building subjected to possible earthquakes from two strike slip faults. The influences of the epistemic uncertainties in source stress drop $\Delta\sigma$ and site attenuation κ_0 on seismic risk are investigated. The need for non-ergodic seismic risk analysis with source-specific and site specific characterizations is emphasized.

Modeling of Fourier amplitude spectra (FAS) of seismic motions has gained much attention in engineering seismology. In the past few years, several ground motion prediction equations (GMPEs) and inter-frequency correlation structure of FAS have been established. Due to many preferable characteristics of FAS, probabilistic seismic hazard/risk analysis is rapidly changing from ergodic, spectrum acceleration $Sa(T_0)$-based approach to non-ergodic, site-specific, FAS-based approach. This paper presents time domain intrusive framework for probabilistic seismic risk analysis using GMPE of FAS. Methodology for time domain stochastic ground motion modeling based on GMPEs of FAS is presented in some detail. The simulated uncertain motions are modeled as a random process and represented by polynomial chaos Karhunen-Loève expansion. The random process excitations are further propagated into the uncertain structural system using Galerkin stochastic finite element method (SFEM). Probabilistic evolution of structural response is solved, and such solution is used to develop seismic risk for any damage state. The presented framework is illustrated through seismic risk analysis of a four-story building subjected to possible earthquakes from two strike slip faults. The influences of the epistemic uncertainties in source stress drop $\Delta\sigma$ and site attenuation κ_0 on seismic risk are investigated. The

need for non-ergodic seismic risk analysis with source-specific and site specific characterizations is emphasized.

Keywords: Seismic risk, Time domain approach, Intrusive stochastic framework, Stochastic Finite Element Method (SFEM), Ground motion prediction equation (GMPE), Fourier Amplitude Spectra (FAS)

1. Introduction

Numerous research efforts in past several decades have established a framework for Performance-based Earthquake Engineering (PBEE) [1–5]. Seismic design has gradually changed from deterministic strength-based design to probabilistic deformation/performance-based design that accounts for all sources of uncertainties in the system [3, 5]. In the probabilistic PBEE framework developed within the Pacific Earthquake Engineering Research Center (PEER), there are four main components [4, 5]:

- Hazard analysis for intensity measure (IM) of ground motions,
- Structural analysis for engineering demand parameter (EDP),
- Damage analysis characterized by damage measure (DM),
- Loss analysis for decision variable (DV).

Traditionally, EDP hazard is computed as the convolution of seismic hazard and structural fragility with respect to intensity measure (IM) of ground motions. Uncertainties in ground motions are represented with the variability of IM through probabilistic seismic hazard analysis (PSHA), while uncertainties in structural systems can be taken into account using fragility analysis. This state of the art approach for seismic risk analysis has been popular in academia and is being adopted in engineering practices [5–7].

Although great progress has been made, there are problems in seismic risk analysis that remain to be solved/improved: First, IM needs to be selected as a proxy of damaging ground shaking on structure systems. Theoretically, the variability of the chosen IM is supposed to represent all the uncertainties in ground motions [8]. However, several researchers [9, 10] pointed out that typical scalar IM, such as spectral acceleration $Sa(T_0)$, could not capture all the uncertainties in seismic motions and could potentially underestimate seismic risk. Luco and Bazzurro [9] and Huang et al. [11], and others[12, 13], have shown that time domain nonlinear analysis with spectrum matched ground motions gives un-conservatively biased risk estimate. It is noted that excellent research advances have been made regarding appropriate IM(s) and ground motion records selection, e.g., averaged spectral acceleration [14, 15], vector IMs [16–20], and hazard-consistent ground motion records selection [21–26], etc.

In conventional seismic risk analysis, Monte Carlo (MC) simulations of structural dynamic responses are required to develop fragility curves using incremental dynamic analysis (IDA) [27]. Monte Carlo (MC) method is a non-intrusive approach that relies on sampling techniques. The underlying deterministic models are iteratively solved with various sampling points of uncertainty [28]. To enhance the computational efficiency of non-intrusive approaches, several advanced Monte Carlo schemes have been developed and used for probabilistic structural analysis, e.g., Latin hypercube sampling [29, 30], quasi-Monte Carlo method [31], and machine learning enhanced approach [32]. In general, MC methods require more samples for reliable tail response estimation [32]. However, this issue is resolved when MC methods are used in conjunction with IM conditioning as in the case IDA. The conditioning IM essentially creates an importance sampling scheme such that only limited number of seismic records and nonlinear time history analyses would be required to accurately capture the conditional variability in the structural response [33].

On the other hand, the authors [34] have established a time domain intrusive approach for probabilistic seismic risk analysis. Compared to the non-intrusive MC method, the intrusive approach directly propagates uncertainties through the engineering system by solving the underlying stochastic models, e.g., stochastic equations of motions in seismic structural analysis [35]. Using the stochastic method [36–39], seismic motions are simulated from stochastic Fourier amplitude spectra (FAS) that is computed with the well-known program SMSIM [40]. Uncertain seismic motions are modeled as a random process in time domain and are applied as stochastic excitations to the uncertain structural system. The probabilistic dynamic structural response is solved for using intrusive Galerkin stochastic finite element method (SFEM) [41, 42]. According to Bazzurro et al. [33], the time domain intrusive approach [34] is a non-conditional approach in the sense that the uncertainties from ground motions are directly propagated into structural systems without IM conditioning. For any non-conditional approach, it is crucial to establish a realistic population of ground motions. The established ground motions set should cover all the important characteristics of seismic motions and their uncertainties that are critical to structural damages. Also, without the IM conditioning and importance sampling scheme from the conditional approach, the non-conditional approach needs to propagate more uncertainties in a holistic way. Therefore, it relies much on efficient uncertainty propagation methods.

Recently, researchers in engineering seismology began to develop and promote GMPEs of Fourier amplitude spectra (FAS) as a substitute for the conventional proxy of seismic motions, spectra acceleration (Sa). FAS is a more direct representation of ground motions than Sa. The scaling of FAS is easier to be related with underlying physics and is better understood from the fundamental seismological theory [43–47]. The relationship between FAS and Sa is systematically studied by Bora et al. [43]. Bora et al. [44, 45] derived GMPEs for FAS using RESOURCE database and NGA-West2 database, respectively. Based on NGA-West2 database, a more sophisticated FAS GMPE, considering rupture depth, hanging wall effects and nonlinear site amplification, was developed by Bayless and Abrahamson [47]. The inter-frequency correlation structure of FAS is also investigated and used for validation of physics-based earthquake modeling [48]. A well-recognized advantage of these empirical FAS models is that, when combined with duration model, adjustment to GMPE of Sa can be easily made for regional/site-specific applications. As envisioned by Abrahamson [49], one of the major changes for seismic hazard/risk analyses in the near future will be the shift from ergodic Sa ground motion models to non-ergodic, site specific FAS models. It is also noted that by combining FAS GMPE with probabilistic model of phase derivative, also known as group delay time [50–54], time domain seismic risk analysis can be performed practically with remarkable simplicity. However, to the best knowledge of the authors', there has not been any seismic risk analysis based on GMPE of FAS. To this end, this paper incorporates several emerging GMPEs [44, 45, 47] of FAS into the time domain intrusive seismic risk analysis framework developed by Wang et al. [34]. The stochastic modeling of uncertain motions are largely simplified with FAS GMPE, making the time domain framework readily applicable for practical seismic risk analysis.

The organization of the paper is as follows: Section 2 summarizes the time domain intrusive seismic risk analysis framework using empirical FAS model. Methodology for time domain uncertain seismic motions modeling based on GMPE of FAS is presented and verified in section 3. Section 4 formulates the general polynomial chaos Karhunen-Loève (PC-KL) expansion uncertainty quantification technique and Galerkin SFEM. The salient features of the proposed framework are illustrated through seismic risk analysis of a four-story shear frame building under potential earthquakes from two strike slip faults in section 5, while conclusions are drawn in section 6.

2. Time Domain Intrusive Seismic Risk Analysis using GMPE of FAS

As illustrated in Figure 1, the proposed framework contains four steps:

1. Seismic source characterization (SSC),
2. Stochastic ground motion modeling,
3. Stochastic finite element analysis and
4. Seismic risk computation.

Seismic source characterization (SSC) part follows the current paradigm in PSHA [55]. Many hazard programs, for example OpenSHA [56] and HAZ45 [57], can perform SSC for a specific site considering epistemic uncertainty/aleatory variability of rupture segmentation, fault slip rate, earthquake recurrence model and magnitude distribution, etc. Regional authorized earthquake rupture forecast (ERF) models can be utilized during SSC, e.g., the model of Third Uniform California Earthquake Rupture Forecast (UCERF3) [58] for California region. A list of seismic scenarios, i.e., different combinations of magnitude M_i and distance R_i and corresponding occurrence rates $\lambda_i(M_i, R_i)$ can be obtained through SSC.

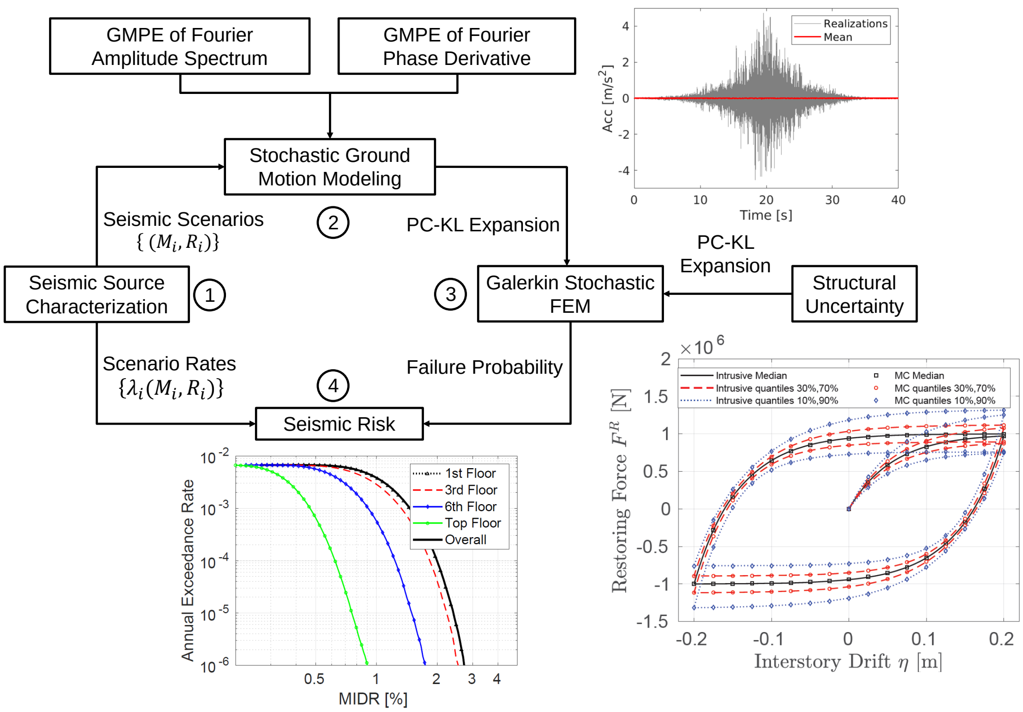

Figure 1: Illustration of the time domain intrusive framework for seismic risk analysis using GMPE of FAS.

For each earthquake scenario, time domain uncertain seismic motions are synthesized from stochastic FAS and Fourier phase spectrum (FPS). FAS is modeled as a Lognormal distributed random field [44, 59] with frequency as the spatial coordinate, whose marginal median and variation behavior are given by emerging GMPEs of FAS [44, 45, 47]. The inter-frequency correlation structure of FAS identified by Bayless and Abrahamson [46] is also adopted. Stochastic FPS is calculated as the integral of probabilistic phase derivative model derived by Baglio [54].

In the third step, synthesized time series realizations of uncertain seismic motions are modeled as a random process and characterized with polynomial chaos Karhunen-Loève (PC-KL) expansion. PC-represented random process seismic motions are intrusively propagated into the uncertain structural system using Galerkin SFEM, that provides complete probabilistic time evolution of the structural response. Probability of undesirable performance $P(EDP > z|M_i, R_i)$ of the selected performance indicator EDP is determined from the probabilistic dynamic structural response.

Finally, if the damage measure (DM) is assumed to be a step function of EDP, seismic risk can be directly calculated by multiplying scenario rate with conditional failure probability and summarizing over all possible scenarios as described by equation 1. For other sophisticated conditional probability relationship $P(DM|EDP)$ between damage measure (DM) and EDP, seismic risk could also be calculated from EDP hazard $\lambda(EDP > z)$ with little effort.

$$\lambda(EDP > z) = \sum_i \lambda_i(M_i, R_i) P(EDP > z|M_i, R_i) \tag{1}$$

The above methodology differentiates from the current PBEE approach in terms of the ground motion interfaces. The current PBEE framework is a conditional approach based on the IM(s) of ground motions. The conditional approach requires proper selection of IM(s) that are well-correlated to structural damages. With the proper IM conditioning in the PBEE framework, smaller conditional variability of structure responses can be quantified with fewer MC time history analysis. On the other hand, for the proposed non-conditional approach, all the uncertainties in the seismic motions are supposed to be well-sampled by a time domain, synthesized population of motions. The selection of structure-specific IM(s) is avoided. However, the non-conditional approach requires reliable time domain ground motion simulation methods such that the generated population could represent all the important characteristics of seismic motions. Furthermore, due to the lack of IM conditioning, the total variability of structural responses quantified by the non-conditional approach is much larger. Propagating such uncertainties using plain Monte Carlo method could be computationally expensive. Therefore, the non-conditional approach has to be used together with efficient uncertainty propagation methods. Specifically in this study, we used GMPE of FAS and FPS to simulate time domain uncertain motions and intrusive Galerkin SFEM for efficient uncertainty propagation.

3. Time Domain Stochastic Ground Motion Modeling using GMPE of FAS

Time domain uncertain motions are inversely Fourier synthesized from stochastic FAS and FPS. The FAS GMPE derived by Bora et al. [44] (referred as Bora15 model hereafter) is adopted for marginal median and standard deviation of Log-normal distributed FAS random field. The proposed framework is general enough to use other FAS GMPEs as well [45, 47]. Multiple FAS GMPEs can be considered with the logic tree approach [60]. In Bora15 model, the input parameters are: Moment magnitude M_w, stress drop $\Delta\sigma$, Joyner-Boore distance R_{JB}, time-averaged shear-wave velocity in upper $30m$ of site V_{S30} and site attenuation parameter κ_0. The uncertain FAS at frequency f follows equation 2,

$$\begin{aligned} lnFAS(f) = c_0 + c_1 M_w + c_2 M_w^2 + c_3 ln(\Delta\sigma) + (c_4 + c_5 M_w) ln(\sqrt{R_{JB}^2 + c_6^2}) \\ -c_7\sqrt{R_{JB}^2 + c_6^2} + c_8 ln(V_{S30}) - c_9\kappa_0 + \delta_{total}(f) \end{aligned} \tag{2}$$

where $c_0 \sim c_9$ are frequency dependent coefficients from regression analysis, and $\delta_{total}(f)$ is the total residual between $ln[FAS(f)]$ and median prediction $ln[\overline{FAS(f)}]$. The total residual $\delta_{total}(f)$ is well-represented as Gaussian distributed random field with zero-mean, marginal standard deviation $\sigma(f)$ and can be decomposed into between event δB , between station $\delta S2S$ and single-station within-event δWS residuals respectively. The $\epsilon(f)$ is the normalization of $\delta_{total}(f)$ by $\sigma(f)$, whose correlation structure $\rho_{\epsilon(f_i),\epsilon(f_j)}$ is found to be important for seismic risk analysis. Neglecting inter-frequency correlation $\rho_{\epsilon(f_i),\epsilon(f_j)}$ would underestimate seismic risk, as noted by Bayless and Abrahamson [46]. Therefore, inter-frequency correlation of $\epsilon(f)$ observed from NGA-West2 records [46, 47] is considered in the FAS modeling as shown in Figure 2.

Stochastic modeling of FPS is another important component. To capture the non-stationarity of seismic motions, phase difference modeling approach was first introduced by Ohsaki [61]. Thráinsson and Kiremidjian [50] modeled phase difference ($\Delta\Phi$) as Beta distribution from 300 California earthquake records. The drawback of using phase difference lies in the instability affected by the seismic signal length. For example, the same record with different signal length (e.g., padding with zeros) would present different distributions of phase difference. Therefore, phase derivative $\dot{\Phi}$ has been adopted as a

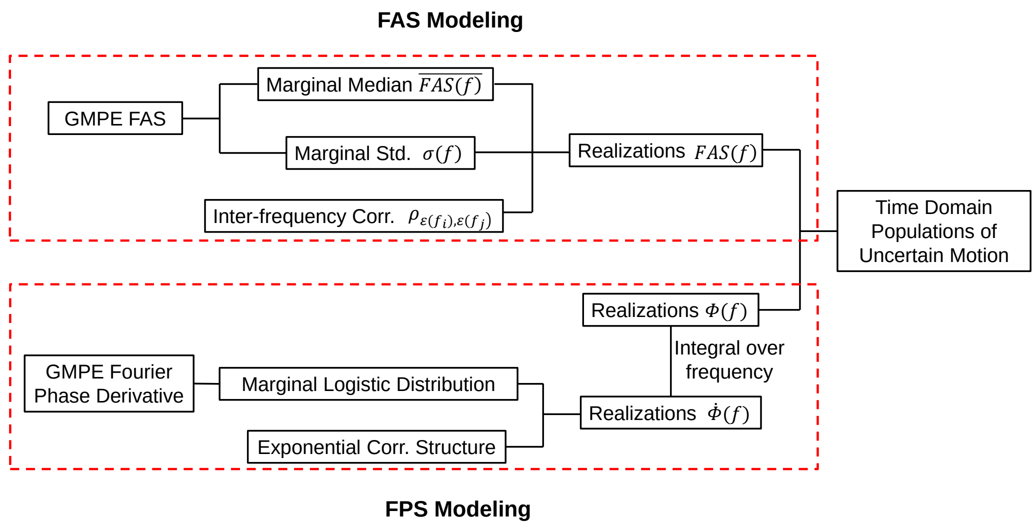

Figure 2: Methodology for time domain stochastic ground motion modeling based on FAS GMPE.

more stable measure for FPS modeling [52–54]:

$$\dot{\Phi} = \frac{\Delta\Phi}{\Delta f} \tag{3}$$

Baglio [54] observed leptokurtic distribution of phase derivative and modeled $\dot{\Phi}$ with Logistic distribution using records in NGA-West database. The dispersion of Logistic distribution is characterized by the scale parameter, which is correlated to the significant duration of ground motions. The GMPE of the scale parameter of phase derivative distribution is established with maximum likelihood estimation [54]. Based on that, Wang et al. [34] simulated time domain stochastic motions using marginal Logistic distributed random phase derivative $\dot{\Phi}(f)$ with exponential inter-frequency correlation structure. Here the same stochastic FPS modeling procedure as Wang et al. [34] is followed. Figure 2 summarizes the proposed methodology for time domain uncertain motion modeling.

Following the methodology, time series realizations of uncertain motions for earthquake scenario $M_w = 7$, $R_{jb} = 12$km from a reverse fault on engineering site with V_{s30}=620m/s are simulated. The stress drop $\Delta\sigma$ is taken as 85 MPa and site attenuation parameter κ_0 is 0.02s [44]. The generated realizations of FAS are shown in Figure 3. From simulated stochastic FAS

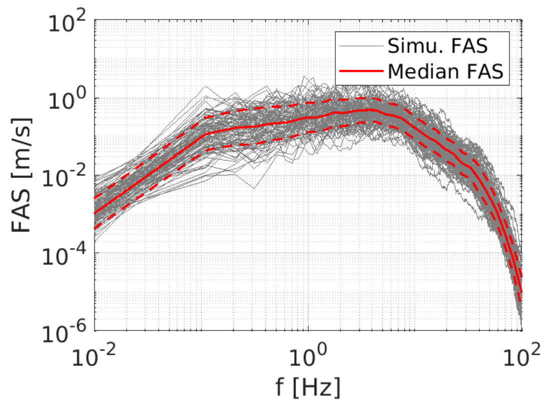

Figure 3: Simulated realizations of log-normal distributed FAS random field with median (red solid line) and $\pm 1\sigma$ (red dashed line) FAS given by GMPE of Bora et al. [44].

and FPS, time series accelerations can be synthesized as shown in Figure 4.

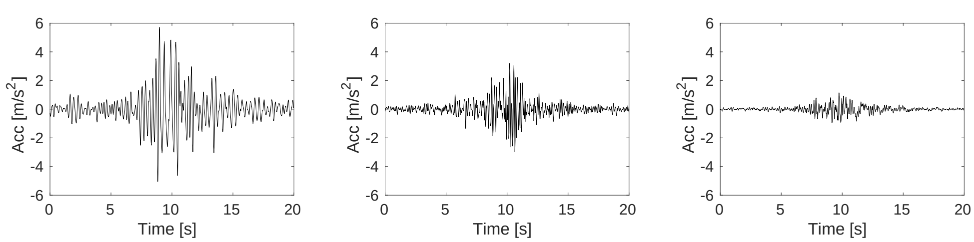

Figure 4: Three realizations of uncertain acceleration time series.

Large variability and non-stationarity are observed. The PGA of simulated time series realizations could vary from 1.3 m/s^2 to 5.8 m/s^2. As shown in Wang et al. [34] and Wang and Sett [62], these uncertain seismic motions can be modeled as a Gaussian distributed random process in time domain. All the desired uncertain seismic characteristics, e.g., Sa, PGA , CAV, etc., are contained in the random process. The use of phase derivative model could capture realistic temporal characteristics of uncertain motions. This is more convenient and accurate than the conventional approach of white noise synthesis where Fourier phase information is forcibly imposed by some envelop modulation functions.

To verify the above methodology for ground motion modeling, spectrum acceleration Sa of the simulated time series are computed and compared with four NGA-West2 GMPEs. From Figure 5(a), it can be seen that the median Sa of simulated time series motions is in good agreement with predictions from GMPEs. In addition, Figure 5(b) shows almost no bias of the simulated median Sa with respect to the weighted average GMPE prediction.

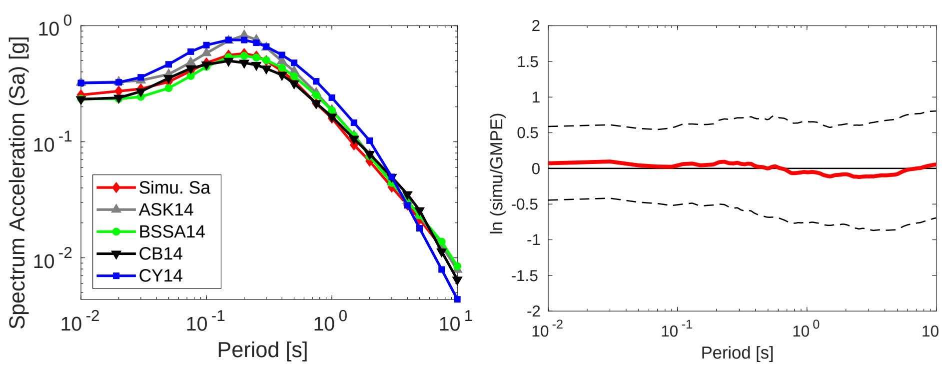

(a) Median Sa comparison with GMPEs

(b) Bias check diagram

Figure 5: Median spectrum acceleration (Sa) of simulated acceleration realizations: (a) Comparison with NGA-West2 GMPEs (b) Bias check, red solid line is the bias of simulated Sa from weighted average GMPEs and dashed lined is $\pm 1\sigma$ simulated Sa.

Figure 6 verifies that the standard deviation (σ) of simulated Sa is also consistent with the variability given by four NGA-West2 GMPEs. Therefore,

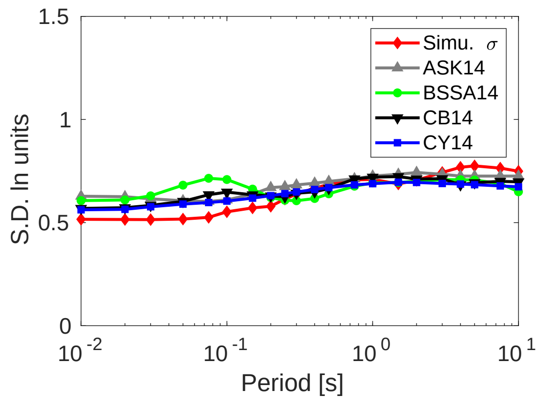

Figure 6: Comparison of aleatory variability of simulated spectrum acceleration (Sa) with NGA-West2 GMPEs.

the presented methodology can synthesize uncertain seismic motions that not only have well-behaved median Sa, but also carry reasonable amount of variability. As mentioned before, it is important for the non-conditional approach to have a realistic non-biased, hazard consistent population of seismic motions. Although the marginal behavior of spectral accelerations are examined, it is still necessary to validate other important aspects of simulated ground motions, e.g., significant duration, Arias intensity and correlation among IMs.

4. Uncertainty Quantification & Galerkin Stochastic FEM

Simulated time histories of seismic motions are regarded as realizations of underlying Gaussian random process. The random process seismic motions, and uncertain structural material parameters are represented by general polynomial chaos Karhunen-Loève (PC-KL) expansion.

Any random process/field $S(\boldsymbol{x}, \theta)$ with general coordinate $\boldsymbol{x}$ can be decomposed with multidimensional Hermite Polynomial Chaos (PCs) given by equation 4,

$$S(\boldsymbol{x}, \theta) = \sum_{i=0}^{P} S_i(\boldsymbol{x}) \Gamma_i(\gamma(\boldsymbol{x}, \theta)) \tag{4}$$

where θ denotes the uncertainty and P is the order of PC [62, 63]. Deterministic PC coefficients is denoted as $S_i(\boldsymbol{x})$ and $\{\Gamma_i\} = \{1, \gamma, \gamma^2 - 1, \gamma^3 - 3\gamma, ...\}$ is zero mean $(i > 1)$, orthogonal Hermite PC basis constructed from kernel zero mean, unit variance Gaussian random field $\gamma(\boldsymbol{x}, \theta)$. The kernel Gaussian random field $\gamma(\boldsymbol{x}, \theta)$ characterizes the correlation structure of the original random process/field $S(\boldsymbol{x}, \theta)$, that is determined from Karhunen-Loève expansion [41, 64] as:

$$\gamma(\boldsymbol{x}, \theta) = \sum_{i=1}^{M} \sqrt{\lambda_i} f_i(\boldsymbol{x}) \xi_i(\theta) \tag{5}$$

In equation 5, M is the dimension of Hermite PC basis. Multidimensional, independent, zero mean, unit variance Gaussian random variables are denoted as $\{\xi_i(\theta)\}$, while λ_i and $f_i(\boldsymbol{x})$ are the eigen-values and eigen-vectors of covariance kernel $Cov_\gamma(x_1, x_2)$ that meet Fredholm's integral equation of the second kind [64, 65]:

$$\int_V Cov_\gamma(x_1, x_2) f_i(x_1)\, dx_1 = \lambda_i f_i(x_2) \tag{6}$$

By combining equations 4 and 5, complete PC-KL representation of general random field $S(\boldsymbol{x}, \theta)$ is obtained, as shown in equation 7.

$$S(\boldsymbol{x},\theta)=\sum_{i=0}^{K}s_i(\boldsymbol{x})\Psi_i(\{\xi_j(\theta)\}) \tag{7}$$

Here $\{\Psi_i\}$ are orthogonal Hermite PC bases in probabilistic space of dimension M, order P. The number of complete Hermite PC bases, according to Ghanem and Spanos [41], is:

$$K=1+\sum_{d=1}^{P}\frac{1}{d!}\prod_{j=0}^{d-1}(M+j) \tag{8}$$

Sakamoto and Ghanem [63] derived the coefficients of multi-dimensional Hermite PC as:

$$s_i(\boldsymbol{x})=\frac{p!}{\langle\Psi_i^2\rangle}S_p(\boldsymbol{x})\prod_{j=1}^{p}\frac{\sqrt{\lambda_{k(j)}}f_{k(j)}(\boldsymbol{x})}{\sqrt{\sum_{m=1}^{M}(\sqrt{\lambda_m}f_m(\boldsymbol{x}))^2}} \tag{9}$$

where p is the order of the polynomial chaos basis Ψ_i. From equation 7, PC synthesized marginal mean, marginal standard deviation and correlation structure of the original heterogeneous random field could be easily calculated [34]. The marginal/joint probabilistic distribution function (PDF) could also be reconstructed with kernel density estimation or Edgeworth's series [41]. By comparing PC-synthesized statistics and PDF with those of the original random field $S(\boldsymbol{x},\theta)$, the goodness of PC-KL expansion can be verified.

Following spatial discretization of deterministic FEM, the weak form of equation of motions for general uncertain dynamic structure systems can be written as [66]:

$$\sum_e \Bigg[\int_{D_e} N_m(\boldsymbol{x})\rho(\boldsymbol{x})N_n(\boldsymbol{x})dV\, \ddot{u}_n(t,\theta) + \\ + \int_{D_e} B_m(\boldsymbol{x})E(\boldsymbol{x},\boldsymbol{\theta})B_n(\boldsymbol{x})dV\, u_n(t,\theta) - f_m(t,\theta)\Bigg] = 0 \quad (10)$$

Here $N_m(\boldsymbol{x})$ is the shape function, while $\rho(\boldsymbol{x})$ is the density field, and $\ddot{u}_n(t,\theta)$ and $u_n(t,\theta)$ denote the uncertain nodal acceleration and displacement, $B_m(\boldsymbol{x})$ is the gradient of the shape function, $E(\boldsymbol{x},\boldsymbol{\theta})$ is the uncertain stiffness field, and $f_m(t,\theta)$ is the uncertain nodal force vector. We apply PC-KL expansion to uncertain stiffness field $E(\boldsymbol{x},\boldsymbol{\theta})$, uncertain nodal force vector $f_m(t,\theta)$ and uncertain nodal responses $u_n(t,\theta)$:

$$E(\boldsymbol{x},\theta) = \sum_{k=0}^{K^E} E_k(\boldsymbol{x})\Psi_k(\{\xi_r(\theta)\}) \quad (11)$$

$$f_m(t,\theta) = \sum_{l=0}^{K^f} f_{ml}(t)\psi_l(\{\xi_r(\theta)\}) \quad (12)$$

$$u_n(t,\theta) = \sum_{l=0}^{K^u} u_{nj}(t)\phi_j(\{\xi_r(\theta)\}) \quad (13)$$

By substituting equations 11, 12 and 13 into equation 10 and applying Galerkin projection [42, 62, 67], spatial-probabilistic discretized weak form equivalent to the original stochastic PDE can be derived:

$$M_{minj}\ddot{u}_{nj} + K_{minj}u_{nj} = F_{mi} \quad (14)$$

where mass tensor/matrix M_{minj}, stochastic stiffness tensor/matrix K_{minj} and stochastic force tensor/vector F_{mi} are given as:

$$M_{minj} = \sum_e \int_{D_e} N_m(\boldsymbol{x})\rho(\boldsymbol{x})N_n(\boldsymbol{x})dV\ \langle\phi_i\phi_j\rangle \quad (15)$$

$$K_{minj} = \sum_{k=0}^{K^E} \sum_{e} \int_{D_e} B_m(\boldsymbol{x}) E_k(\boldsymbol{x}) B_n(\boldsymbol{x}) dV \ \langle \Psi_k \phi_i \phi_j \rangle \tag{16}$$

$$F_{mi} = \sum_{l=0}^{K^f} f_{ml} \langle \psi_l \phi_i \rangle \tag{17}$$

In equations 15, 16 and 17, symbol $\langle \cdot \rangle$ represents the expectation operator, $\Psi_k(\{\xi_r(\theta)\})$, $\psi_l(\{\xi_r(\theta)\})$ and $\phi_j(\{\xi_r(\theta)\})$ are the PC bases of uncertain stiffness, uncertain forces and uncertain structural response, respectively, $\langle \phi_k \phi_m \rangle$, $\langle \psi_j \phi_m \rangle$ and $\langle \Psi_i \phi_k \phi_m \rangle$ are the ensemble average tensors of double-product and tri-product of Hermite PC bases.

Equation 14 becomes a deterministic ODE system of unknown PC coefficients u_{nj}. This equation could be solved using any temporal, time marching integration scheme, for example, Newmark method [68]. For more detailed formulations and verification of stochastic FEM, please refer to Wang et al. [34], Ghanem and Spanos [41], Sett et al. [42], Wang and Sett [62], Deb et al. [67], Matthies and Keese [69].

Probabilistic evolution of the displacement response can then be constructed through the solved PC coefficients u_{nj}. From the probabilistic displacement response, failure probability $P(EDP > z|M_i, R_i)$ can be calculated and used further for risk computation.

5. Illustrative Example

To illustrate the presented time domain intrusive framework using GMPE of FAS, seismic risk of a four-story building subjected to potential earthquakes from two strike slip faults is analyzed. The configuration of two faults and the target engineering site is shown in Figure 7(a). Fault 1 is parameterized based on San Gregorio fault [58] in California. San Gregorio fault is comprised of northern section (129km) and southern section (89km). The

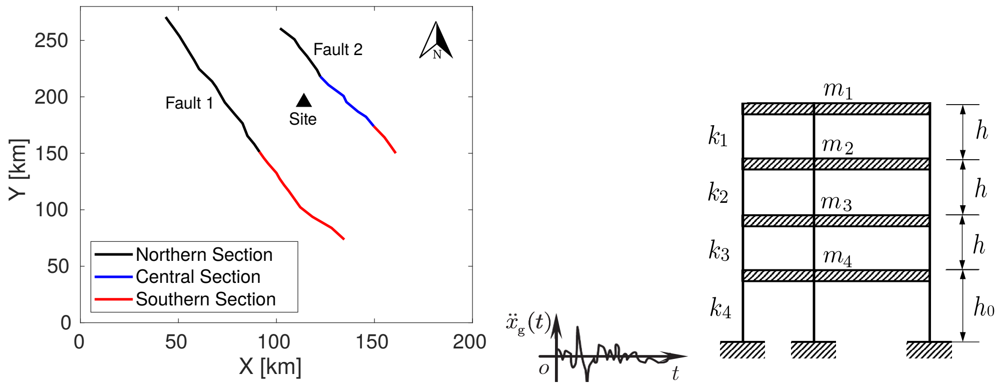

(a) Faults configuration (b) Building structure

Figure 7: Configuration of faults, site and engineering structures: (a) Engineering site (black triangle) at (114km, 174km) with $Vs_{30} = 620m/s$ and two nearby strike slip faults (b) Four-story building structure with uncertain stiffness field located at the engineering site (black triangle).

parameters of Fault 2 are determined with reference to Calaveras fault [58] in California. Calaveras fault is comprised of northern section (48km), central section (52km) and southern section (26km). The target engineering site is located at coordinates x =114km, y =174km, closer to Fault 2, with the site condition represented through shear wave velocity of $V_{s30} = 620$m/s. A four-story building is located at the site, as shown in Figure 7(b). Building has a deterministic floor mass $m = 100$ kips/g and uncertain elastic story stiffness field k. The uncertain story stiffness k is modeled as Lognormal distributed random field with marginal median $\overline{k} = 168$ kip/in and marginal standard deviation $0.1 ln$ units. The correlation structure of the story stiffness random field k is assumed to be exponential with correlation length $l_c = 3$ floors. It is noted that only a linear elastic structure was used in this study for illustrative purposes. For realistic structures with nonlinear behavior, the presented intrusive SFEM can be extended to stochastic elastoplastic FEM

(SEPFEM) [42] with additional formulations of probabilistic elastoplasticity [35, 70]. Using the intrusive SEPFEM, the development of the probabilistic elastic-plastic stiffness at the constitutive level could be challenging for some complex nonlinear behavior. Some least square optimization and linearization techniques [35, 42] could be used. Meanwhile, it requires further developments of SEPFEM to model structural collapse. On the other hand, there are also some non-intrusive uncertainty propagation techniques, e.g., regression-based polynomial chaos expansion [71] and stochastic collocation [72]. These methods could handle complex nonlinear structural behavior and collapse response with superior computational performance compared to the standard MC method.

5.1. Seismic Source Characterization

Following the methodology presented in Section 2, in Figure 1, seismic source characterization (SSC) is the first step to quantify all the possible earthquake scenarios, including magnitudes, distances, and corresponding occurrence rates. Only earthquakes with magnitude greater than 5.0 are considered here. The extensively verified hazard program HAZ45 [57] is used for SSC. The rupture segmentation model, geometry, characteristic magnitude and annual slip rate of these two faults are determined from the investigation of San Gregorio and Calaveras fault by Field et al. [58] and Thomas et al. [73]. Table 1 summarizes these input parameters for HAZ45. The epistemic uncertainty for alternative segmentation models, rupture widths, characteristic magnitudes and slip rates are considered with the logic tree approach [60]. The weights for logic tree branches are given inside the brackets in Table 1.

In addition, two alternative probabilistic magnitude distribution models are adopted in SSC: (a) Youngs and Coppersmith model [74] and (b) trun-

Table 1: Source characterization with epistemic uncertainty: Parameters for Fault 1 and Fault 2 are based on San Gregorio and Calaveras fault in California according to Field et al. [58] and Thomas et al. [73].

Fault Name	Rupture Scenario	Segment	Rupture Length [km]	Rupture Width [km]	Characteristic Magnitude	Slip Rate [mm/yr]
Fault 1	Unsegmented (0.35)	Northern & Southern Section	218	11 (0.3) 13 (0.4) 15 (0.3)	7.2 (0.2) 7.5 (0.6) 7.8 (0.2)	1 (0.1) 3 (0.4) 5 (0.4) 7 (0.1)
	Segmented (0.35)	Northern Section	129	11 (0.3) 13 (0.4) 15 (0.3)	6.9 (0.2) 7.2 (0.6) 7.5 (0.2)	2 (0.2) 5 (0.6) 7 (0.2)
		Southern Section	89	10 (0.3) 12 (0.4) 14 (0.3)	6.7 (0.2) 7.0 (0.6) 7.3 (0.2)	1 (0.2) 2 (0.6) 3 (0.6)
	Floating Earthquake (0.3)	Northern & Southern Section	218	11 (0.3) 13 (0.4) 15 (0.3)	6.6 (0.2) 6.9 (0.6) 7.2 (0.2)	1 (0.1) 3 (0.4) 5 (0.4) 7 (0.1)
Fault 2	Unsegmented (0.1)	Whole Fault	126	9 (0.3) 11 (0.4) 13 (0.3)	6.9 (0.2) 7.2 (0.6) 7.5 (0.2)	4 (0.1) 6 (0.4) 10 (0.4) 14 (0.1)
	Two Segments (0.5)	Northern Section	48	11 (0.3) 13 (0.4) 15 (0.3)	6.6 (0.2) 6.9 (0.6) 7.2 (0.2)	4 (0.2) 5 (0.6) 6 (0.2)
		Central & Southern Section	78	9 (0.3) 11 (0.4) 13 (0.3)	6.7 (0.2) 7.0 (0.6) 7.3 (0.2)	6 (0.1) 10 (0.4) 12 (0.4) 14 (0.1)
	Three Segments (0.3)	Northern Section	48	11 (0.3) 13 (0.4) 15 (0.3)	6.6 (0.2) 6.9 (0.6) 7.2 (0.2)	4 (0.2) 5 (0.6) 6 (0.2)
		Central Section	52	9 (0.3) 11 (0.4) 13 (0.3)	6.5 (0.2) 6.8 (0.6) 7.1 (0.2)	6 (0.2) 10 (0.6) 14 (0.3)
		Southern Section	26	9 (0.3) 10 (0.4) 11 (0.3)	6.2 (0.2) 6.5 (0.6) 6.8 (0.2)	9 (0.2) 12 (0.6) 15 (0.2)
	Floating Earthquake (0.1)	Whole Fault	126	9 (0.3) 11 (0.4) 13 (0.3)	6.5 (0.2) 6.8 (0.6) 7.1 (0.2)	4 (0.1) 6 (0.4) 10 (0.4) 14 (0.1)

cated normal distribution with weights 0.7 and 0.3, respectively. For the numerical integration in HAZ45, the discretization step is 0.2 for magnitude and 2km for distance. A list of 371 different earthquake scenarios are generated for San Gregorio fault with magnitude $M_w = 5.1 \sim 8.3$ and distance $R_{jb} = 38\text{km} \sim 120\text{km}$. For Calaveras fault, there are 182 different seismic scenarios with magnitude $M_w = 5.1 \sim 7.9$ and distance $R_{jb} = 19\text{km} \sim 63\text{km}$. By combining scenarios from San Gregorio and Calaveras fault, the distribution of all possible scenarios for the engineering site is shown in Figure 8. It can be seen that the dominant scenarios for the site are magnitude

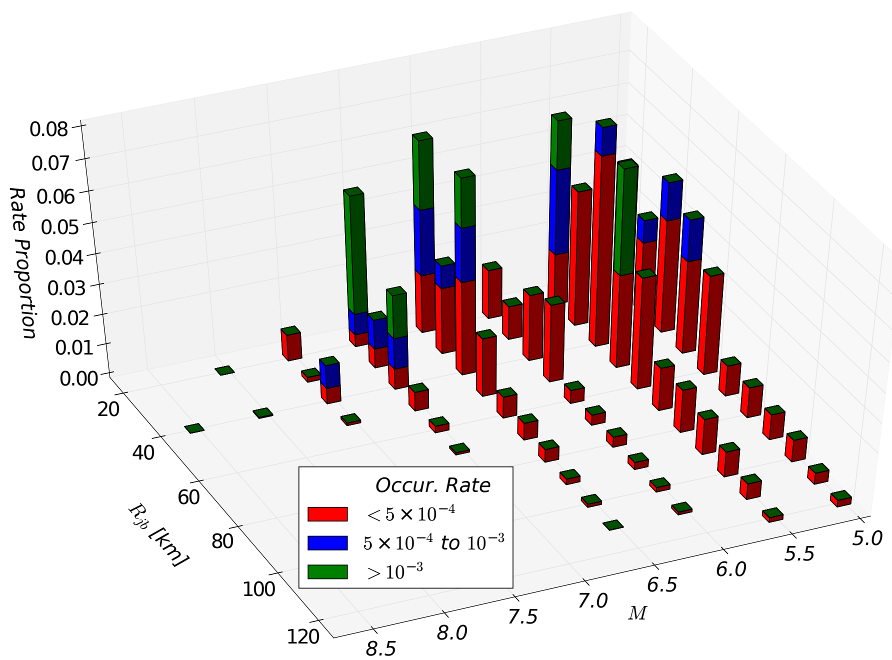

Figure 8: Distribution of all the possible earthquake scenarios for the engineering site.

$M_w = 5 \sim 5.5$ and $M_w = 6.5 \sim 7.0$, and distance $R_{jb} = 20\text{km} \sim 40\text{km}$.

5.2. Stochastic Ground Motion Modeling & PC-KL Representation

For each scenario, the marginal median and standard deviation of the Lognormal distributed FAS random field are determined using Bora15 GMPE of FAS [44]. Time series realizations of uncertain motions are synthesized from stochastic FAS and FPS following the verified methodology in section 3. The uncertain motions are modeled as Gaussian random process in time domain. With simulated realizations of the underlying Gaussian random process, the random process can be represented with multidimensional Hermite PCs using PC-KL expansion technique derived in section 4. Here the lognormal distributed stiffness random field is characterized with PCs of dimension 4, order 2, while the Gaussian random process motions are characterized with PCs of dimension 150, order 1. Choosing appropriate order of PCs is important to quantify the non-Gaussianity of the stiffness field. The appropriate number of PC dimensions is also crucial to capture the correlation structure of the random process motions, as shown in Figure 9. For detailed discussion

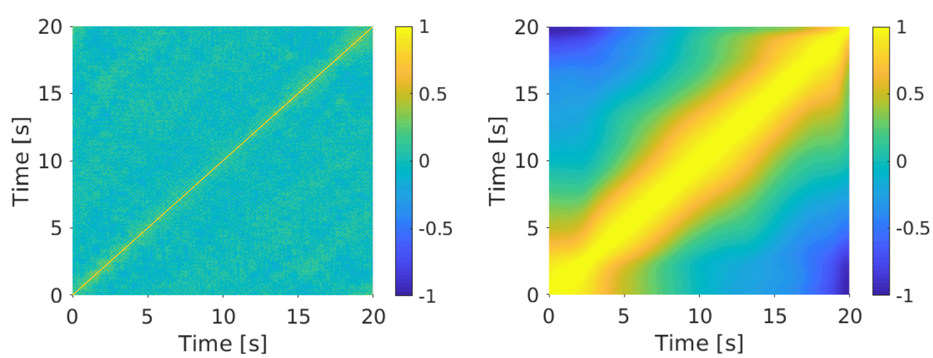

(a) Acceleration (b) Displacement

Figure 9: Correlation structure of random process seismic motions: (a) Acceleration (b) Displacement.

about PC-KL representation with different order and dimension of PCs for the uncertain motion and the uncertain stiffness field, please refer to Wang et al. [34] and Wang and Sett [62].

5.3. Dynamic probabilistic structural response with Galerkin SFEM

The uncertain structural system excited by uncertain motions would produce probabilistic dynamic displacement responses. Probabilistic dynamic displacement response is also PC-KL expanded in probabilistic space. The deterministic unknown PC coefficients, which contain all the information about the probabilistic evolution of displacement responses, are solved for using Galerkin SFEM formulated in Section 4. Using resulting PC coefficients, probabilistic evolution of any engineering demand parameters (EDP), for example, relative floor deformation and inter-story drift ratio, can be constructed. Figure 10 shows the time evolving mean and standard deviation of relative deformation of different floors to the ground under uncertain seismic excitations from the earthquake scenario $M_w = 7.5$ and $R_{jb} = 38km$. The

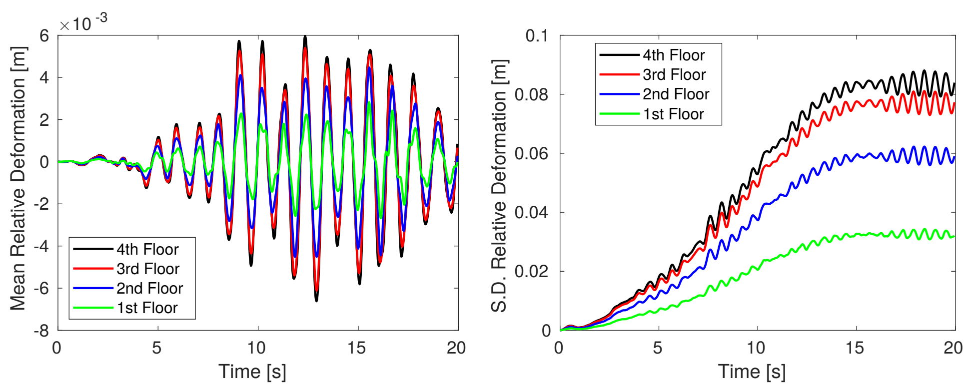

(a) Mean (b) Standard deviation

Figure 10: Time evolving mean and standard deviation (S.D.) of relative deformation of floors under uncertain seismic excitations from earthquake scenario $M_w = 7.5$, $Rjb = 38km$.

mean relative deformation is generally very small. From Figure 10(b), it can be observed that the standard deviation of relative deformation between different floors increases with the height and reaches the maximum at the top floor.

The deformation of the building at four different times, $t = 5s, 10s, 15s$ and $20s$ is shown in Figure 11, where solid lines with diamond marker depict the mean deformation while dashed lines with circle marker give the $\pm 1\sigma$ deformation limit. As time proceeds, the structural deformation generally

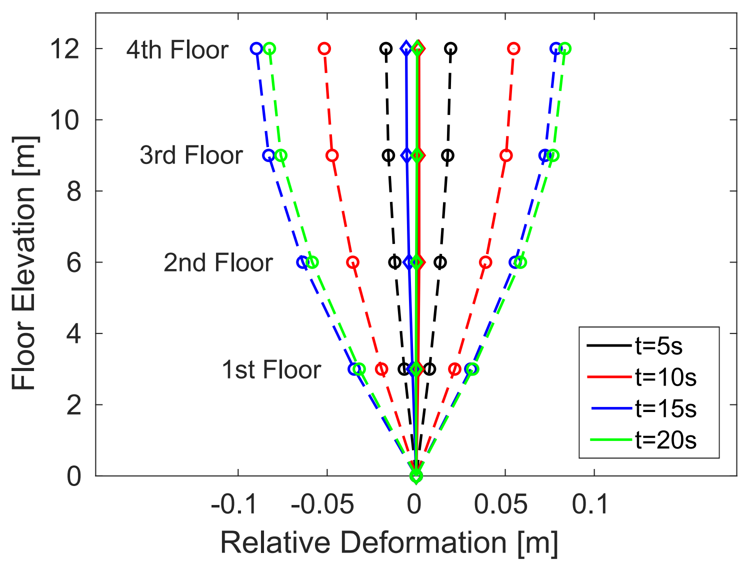

Figure 11: Dynamic probabilistic deformation of the four-story building: Solid line with diamond markers represents the mean relative displacement; Dashed line with circle markers represents $\pm 1\sigma$ deformation limit.

becomes more uncertain and wider, as $\pm 1\sigma$ of deformation shows.

The maximum inter-story drift ratio (MIDR) is chosen as EDP for risk analysis. The evolution of PDF for MIDR among four floors is shown in

Figure 12. The dispersion and shift of median response of MIDR along the

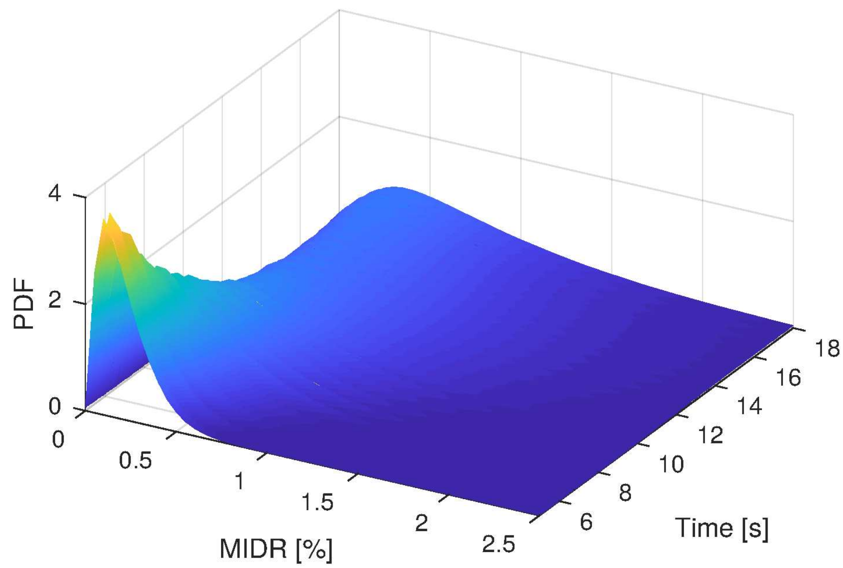

Figure 12: Time-evolving probabilistic distribution of MIDR among four floors.

time can be observed.

The PDF of overall MIDR among four floors and throughout the time is plotted as the black, full line, curve in Figure 13. The PDFs for MIDR of individual floor throughout the time are also shown in Figure 13 for comparison. The distribution of MIDR for the top floor (i.e., the 4th floor) shows the minimum median behavior and the narrowest dispersion. In contrast, the distribution of MIDR for the first floor overlaps with the PDF of the overall MIDR, showing the largest median and the widest dispersion.

Since the PDF of overall MIDR is crucial to compute the failure probability $P(EDP > z)$, comparative studies have been conducted to investigate how different scenarios would influence the distribution of MIDR. Five specific earthquake scenarios are picked out from the total number of 553 possible scenarios and listed in Table 2.

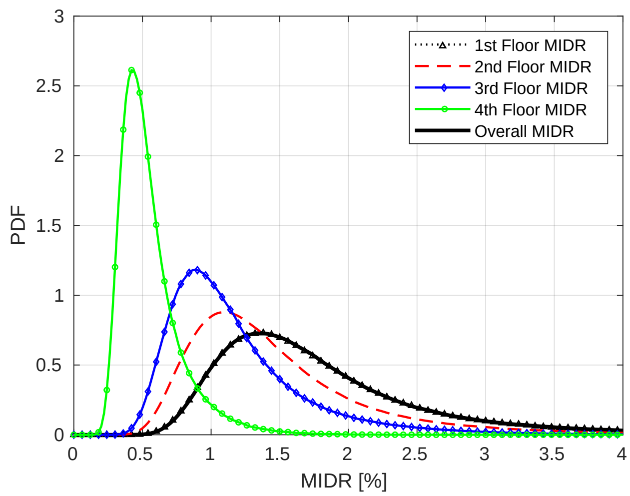

Figure 13: PDF of MIDR throughout the time for the whole structure and individual floor under earthquake scenario $M_w = 7.5$, $R_{jb} = 38km$.

Table 2: Scenarios for comparative studies of different magnitudes and distances: Fault 1 and Fault 2 are based on San Gregorio and Calaveras faults in California.

Scenario ID	Magnitude	Distance [km]	Rupturing Fault	Annual Rate [/yr]
1	6	50	Fault 1	5.09×10^{-5}
2	6.5	50	Fault 1	5.09×10^{-5}
3	7	50	Fault 1	1.01×10^{-4}
4	6.5	20	Fault 2	9.75×10^{-4}
5	6.5	100	Fault 1	8.51×10^{-6}

Scenarios No. 1, 2 and 3 in Table 2 have the same distance $R_{jb} = 50km$ but different magnitudes $M_w = 6$, 6.5 and 7. Scenarios No. 2, 4 and 5 in Table 2 have the same magnitude $M_w = 6.5$ but different distances $R_{jb} = 20km$, $50km$ and $100km$. Figure 14 shows the resultant PDFs of overall MIDR for these scenarios. From Figure 14(a), it can be observed that as the

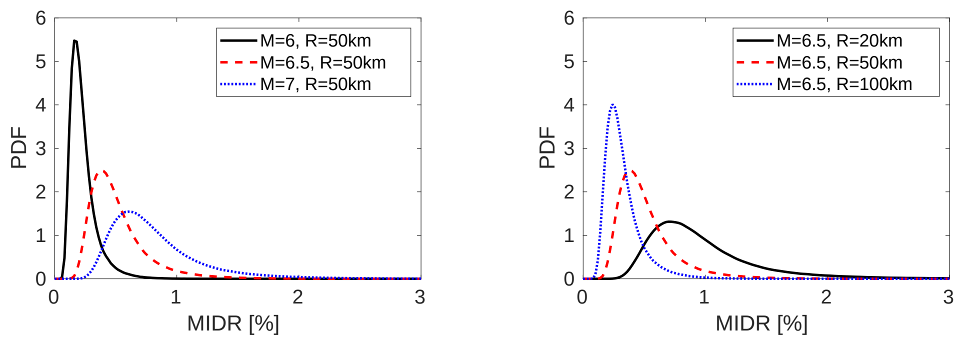

(a) Different magnitudes

(b) Different distances

Figure 14: PDF of MIDR with varying magnitudes and distances.

magnitude increases, the median of MIDR distribution shifts to the right and demonstrates larger dispersion. Figure 14(b) shows the same trend when the scenario distance decreases.

The exceedance probability of MIDR $P(\text{MIDR} > z)$ is calculated as the complementary cumulative distribution function (CCDF) of MIDR distribution. Multiplying the exceedance probability with the corresponding scenario rate given in Table 2, EDP hazard $\lambda(\text{MIDR} > z)$ caused by the individual earthquake scenario is obtained. Figure 15 shows the EDP hazard curves for the five earthquake scenarios in Table 2. In Figure 15, different levels of plateau in EDP hazard curves are observed because of the differences in scenario rates. The shift of bending point in EDP hazard curves with varying

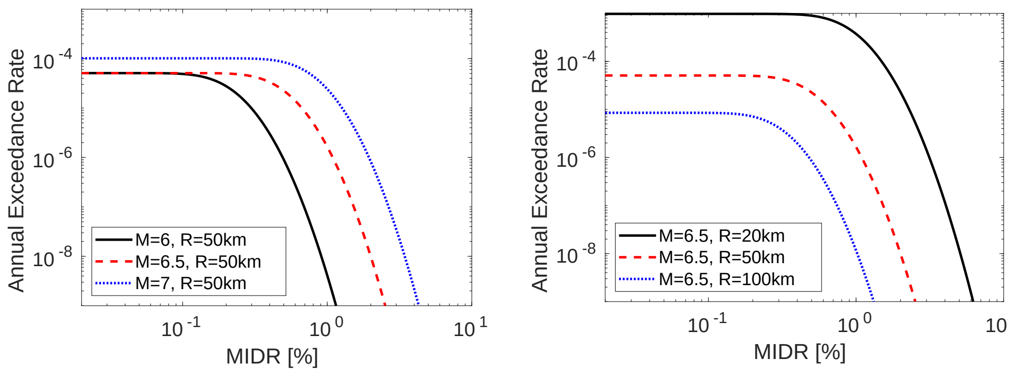

(a) Different magnitudes

(b) Different distances

Figure 15: Annual exceedance rate of MIDR with varying magnitudes and distances.

magnitude and varying distance is consistent with the shift of median MIDR shown in Figure 14.

5.4. Seismic risk and risk de-aggregation

Adding up EDP hazard from the individual seismic scenario, the total EDP hazard for the engineering site and hazard contribution from Fault 1 and Fault 2 are calculated and shown in Figure 16. Then damage measure (DM) is used to quantify the physical damage condition of the engineering system. Theoretically, DM could be defined as very complicated criteria of single or multiple EDPs. However, there is still a knowledge gap to characterize all the necessary DMs and corresponding DM-EDP(s) relations [4]. In engineering practices, simplified criteria of DM is commonly used. For example, FEMA-365 [75] defines collapse damage state for code-conforming reinforced concrete buildings as inter-story drift ratio greater than 4%. Similarly, in this paper, we consider three different damage states by assuming DM as a step function of the selected EDP, i.e., maximum inter-story drift ratio (MIDR) greater

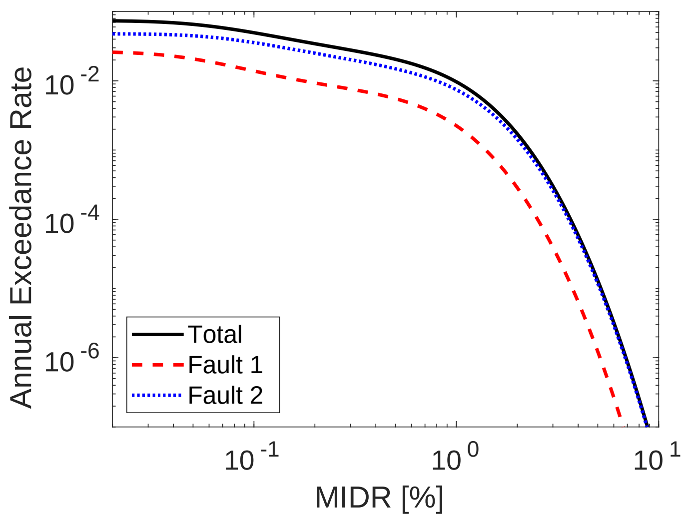

Figure 16: Annual exceedance rate of MIDR: Fault 1 and Fault 2 are based on San Gregorio and Calaveras faults in California.

than 1%, 2% and 4%. By assuming DM as a step function of EDP, seismic risk values for damage states with MIDR exceedance of 1%, 2% and 4% can be easily found from Figure 16 as 9.7×10^{-3}, 1.7×10^{-3} and 5.9×10^{-5}, respectively. It is noted that the simplified definition of damage measure will lead to some inaccuracy for seismic risk analysis. The risk values for damage states defined by different damage measures could be very different. There are many ongoing research on the accurate DM-EDP(s) relationships for seismic risk analysis [76–78]. However, this issue is beyond the scope of this paper.

The contribution from individual scenarios to the total seismic risk can also be de-aggregated. Figure 17 presents the de-aggregation of seismic risk for MIDR exceeding 1%. From Figure 17, it is clear that the seismic risk is controlled by earthquakes from Fault 2 with magnitude $M_w = 6.5 \sim 7.0$ and distance $R_{jb} = 20$km.

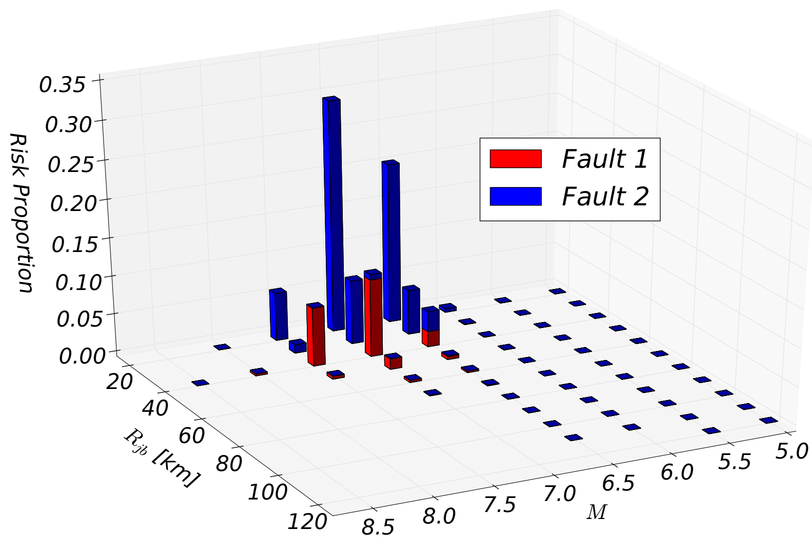

Figure 17: De-aggregation of seismic risk for MIDR exceeding 1%.

These derived risk curves can be used further for loss analysis and provide insights for performance-based seismic design of new buildings and retrofit of existing buildings. The controlling seismic scenarios from the de-aggregation of risk curves could also be used to guide earthquake emergence preparedness and response.

5.5. Sensitivity study on earthquake stress drop $\Delta\sigma$ and site attenuation κ_0

For the stochastic ground motion modeling in this study, stochastic FAS are governed by Bora15 GMPE of FAS [44]. Besides some common input parameters (e.g., M_w, R_{jb}, V_{s30}), Bora15 GMPE of FAS also takes inputs for source stress drop $\Delta\sigma$ and near site anelastic attenuation κ_0. Since source specific $\Delta\sigma$ and site specific κ_0 are generally not available in engineering practices, ergodic assumption is typically made: Regional, ergodic estimates of stress drop $\Delta\sigma$ and anelastic attenuation κ_0 are used and it is assumed that these estimates are uniformly applicable to all sources and sites within the region. For example, in California, regionally ergodic estimates could be 5MPa for stress drop $\Delta\sigma$ and 0.025s for anelastic attenuation κ_0 [79].

The sacrifice for the ergodic assumption is to use relatively large total standard deviation for variability, which incorporates source to source variability (τ), site to site variability (ϕ_{s2s}) and within site variability (ϕ_{ss}). Furthermore, it is still not quite clear how the epistemic uncertainty of these ergodic estimates, i.e., different inputs of $\Delta\sigma$ and κ_0, could influence the seismic risk.

To answer this question, sensitivity study on different GMPE inputs of stress drop $\Delta\sigma$ and anelastic attenuation κ_0 is presented. Seismic risks for the controlling scenario $M_w = 7.0$, $R_{jb} = 20km$ from risk de-aggregation are computed with different $\Delta\sigma$ and κ_0 estimates. Figure 18(a) shows three EDP hazard curves with different stress drop values $\Delta\sigma$ =1MPa, 5MPa and 15MPa, while anelastic attenuation is kept at the same value of $\kappa_0 = 0.02$s.

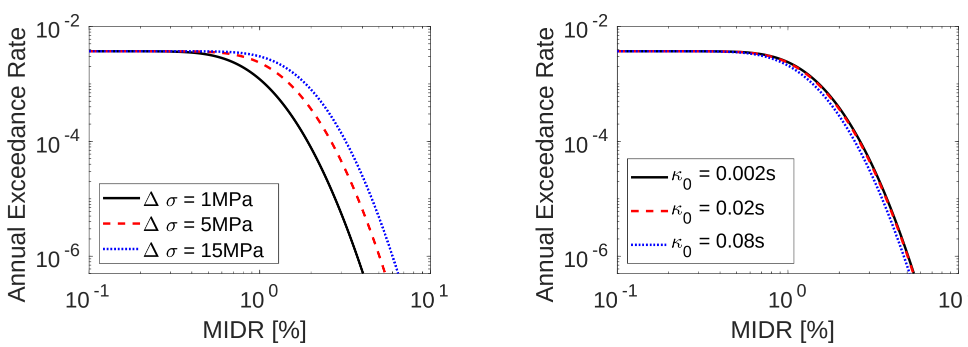

(a) Different stress drops $\Delta\sigma$ (b) Different anelastic attenuation κ_0

Figure 18: Sensitivity analysis of annual exceedance rate of MIDR with varying source parameter $\Delta\sigma$ and site parameter κ_0 for seismic scenario $M_w = 7$, $R_{jb} = 20km$.

With the increase of stress drop, significant shift of EDP hazard curve to the right can be seen. Because of the shift, seismic risk for damage state with MIDR exceedance of 1% is 3×10^{-3} for $\Delta\sigma = 15$MPa, which is larger than the risk value 2.3×10^{-3} for $\Delta\sigma = 5$MPa and 1.2×10^{-3} for $\Delta\sigma = 1$MPa. For seismic risk of 2% MIDR exceedance, the difference is even more significant: Seismic risk for $\Delta\sigma = 15$MPa is 7.97×10^{-4} and is around 10 times the risk value 7.71×10^{-5} for $\Delta\sigma = 1$MPa. Therefore, it is crucial to conduct source specific characterization of stress drop $\Delta\sigma$ for more accurate risk quantification. Great needs for non-ergodic ground motion modeling and seismic hazard/risk analysis are emphasized [80].

Compared with the stress drop $\Delta\sigma$, in this case the seismic risk is not very sensitive to the variation of the site attenuation parameter κ_0. In Figure 18(b), sensitivity of EDP hazard with respect to the variation of κ_0 is shown. Stress drop $\Delta\sigma$ is kept as 5MPa, while three different values of site attenuation parameter κ_0 are adopted as $\kappa_0 = 0.002s$, $0.02s$ and $0.08s$. It can be seen that three EDP hazard curves for $\kappa_0 = 0.002s$, $0.02s$ and $0.08s$ almost overlap with each other. The epistemic uncertainty of κ_0 in this case would not have notable influence on the final seismic risk. This suggests that for this specific case, more resources (time, money, etc.) could be spent on seismic source characterization instead of investigating near site attenuation.

The fundamental causes for different sensitivity response of stress drop $\Delta\sigma$ and site attenuation κ_0 are revealed in Figure 19. Median FAS given by Bora15 GMPE of FAS [44] with varying stress drop $\Delta\sigma$ and site attenuation κ_0 are presented. From the FAS, the dominant frequencies for seismic motions are between 0.1Hz $\sim$ 4Hz. As shown in Figure 19(a), difference in stress drop could produce significantly different Fourier amplitude ordinates for frequencies greater than 0.1Hz, which would generate time domain uncertain motions with distinct amplitudes.

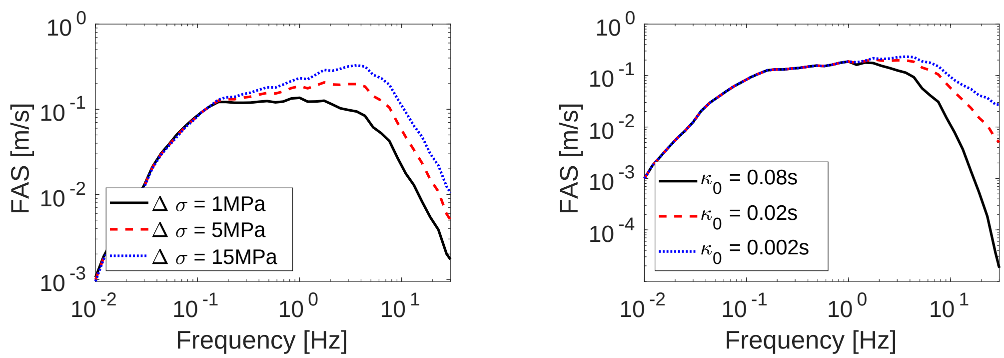

(a) Different stress drops $\Delta\sigma$ (b) Different anelastic attenuation κ_0

Figure 19: Sensitivity analysis of median FAS with varying source parameter $\Delta\sigma$ and site parameter κ_0 for seismic scenario $M_w = 7$, $R_{jb} = 20km$.

In contrast, Figure 19(b) shows that variation of near site attenuation κ_0 would only influence high frequency portion ($f > 3$Hz) of the motions. The dominant parts of FAS for this case are not much influenced by the differences in site attenuation κ_0. Furthermore, it is noted that the fundamental frequency of the four-story building is 1.6Hz calculated with the median story stiffness. Fourier amplitude ordinates around 1.6Hz vary notably with different stress drops $\Delta\sigma$, while the ordinates stay almost unchanged with varying site attenuation κ_0. Therefore, in this case Fourier synthesized motions using different site attenuation κ_0 would not lead to much difference in the final seismic risk.

It is important to note, based on the above analysis, that in some other cases, site attenuation κ_0 could be important for seismic risk. For example, in central and eastern USA, seismic motions are rich in high frequency (HF) contents, site attenuation introduced by different κ_0 values could significantly influence the amplitude of motions propagating into structural systems. For some critical structures sensitive to high frequency excitations, e.g., nuclear power plants, accurate characterization of κ_0 could also be of great importance. To confirm this, the median story stiffness of the original building is increased from 168kip/in to 840kip/in and the floor mass is reduced from 100kips/g to 20kips/g. The fundamental frequency of the building changes from 1.6Hz to 8Hz. The EDP hazard curves for the new building structure with varying site attenuation (κ_0) values are given in Figure 20.

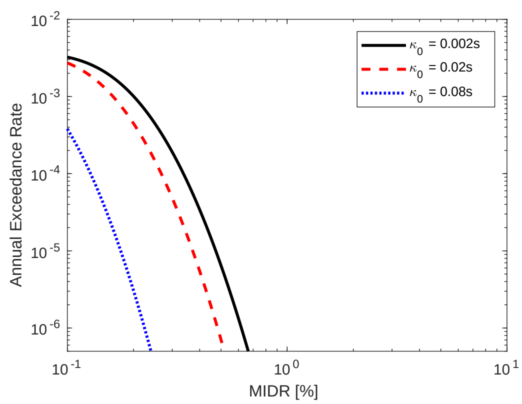

Figure 20: Annual exceedance rate of MIDR with varying attenuation parameter κ_0 for a stiffer structure (fundamental frequency 8Hz) under seismic scenario $M_w = 7$, $R_{jb} = 20km$.

In contrast to Figure 19(b), for such a stiffer structure with much higher fundamental frequency, strikingly different seismic risks are obtained for different values of site attenuation κ_0. This urges the use of refined, site-specific site attenuation κ_0 for seismic risk analysis of structures susceptible to high frequency shaking, especially for those structures in central and eastern USA.

6. Conclusions

Presented is a time domain intrusive framework for probabilistic seismic risk analysis using GMPE of FAS. FAS, as the fundamental characteristic of seismic motions, has become popular in engineering seismology. Compared with traditional intensity measures, e.g., spectral acceleration Sa, FAS provides a more direct representation of ground motions and has clear scaling behavior related to the underlying earthquake physics. Using FAS, it is more convenient to develop time domain, non-ergodic region/site-specific seismic motions. Compared with stochastic modeling of FAS using SMSIM [34, 40], GMPE FAS is better calibrated and more consistent with observed seismic records. The time domain uncertain ground motions modeling is greatly simplified with FAS GMPE, which makes the whole risk analysis methodology applicable for engineering practices.

Seismic risk of a four-story building under potential earthquakes from two faults is analyzed with the presented framework. The presented method is a non-conditional approach for risk analysis. A population of simulated time domain seismic motions is used to capture the uncertainties in ground motions. The method does not require the selection of IM. However, the method requires reliable time domain ground motion simulation approaches such that the generated population could represent all the important characteristics of seismic motions. In this paper, stochastic time domain ground motions are simulated from the GAMPEs of FAS and FPS. The uncertain seismic motions are directly propagated into the uncertain structure system in a holistic way without IM conditioning. Compared to the importance sampling scheme in the conditional approach, larger variability in the structural response needs to be quantified in the proposed non-conditional approach. Using standard Monte Carlo method for uncertainty propagation in this case would be computationally expensive. Therefore, intrusive stochastic FEM is formulated for efficient uncertainties propagation. The complete probabilistic dynamic structural response is solved through stochastic FEM. The probability distribution, hazard/risk of any chosen EDP(s) is computed by post-processing the probabilistic structural response. Sensitivity studies show that EDP hazard could significantly change with different estimates of source stress drop. For structures with relatively low fundamental frequency, the influence of site attenuation κ_0 on seismic risk is not as significant as is the influence of stress drop $\Delta\sigma$. This is particularly true when seismic motions are dominated with low and medium frequency contents. However, for structures sensitive to high frequency motions, great emphasis should be put on accurate characterization of site attenuation κ_0. Need for non-ergodic seismic hazard/risk analysis with source-specific, site-specific characterization is demonstrated for reliable risk estimates.

Some aspects in the presented framework still need improvement. Future work includes further validation of the presented time domain ground motion simulation method for other seismic characteristics, developing better Fourier phase derivative models with near field motion characteristics and applying the method to more realistic structures with complex nonlinear behavior. Presented methodology is implemented and available within the Real-ESSI Simulator [81].

7. Acknowledgments

Presented research was primarily funded from the private sources, from the University of California and in small part the US-DOE.

References

[1] C. Allin Cornell. Engineering seismic risk analysis. *Bulletin of the seismological society of America*, 58(5):1583–1606, 1968.

[2] C. Allin Cornell and Helmut Krawinkler. Progress and challenges in seismic performance assessment. *PEER newsletter*, 2000. https://apps.peer.berkeley.edu/news/2000spring/performance.html Accessed 1 August 2018.

[3] Ahmed Ghobarah. Performance-based design in earthquake engineering: state of development. *Engineering structures*, 23(8):878–884, 2001.

[4] Jack Moehle and Gregory G Deierlein. A framework methodology for performance-based earthquake engineering. In *13th world conference on earthquake engineering*, volume 679, 2004.

[5] Selim Günay and Khalid M Mosalam. PEER performance-based earthquake engineering methodology, revisited. *Journal of Earthquake Engineering*, 17(6):829–858, 2013.

[6] Paulos B Tekie and Bruce R Ellingwood. Seismic fragility assessment of concrete gravity dams. *Earthquake engineering & structural dynamics*, 32(14):2221–2240, 2003.

[7] John B Mander, Rajesh P Dhakal, Naoto Mashiko, and Kevin M Solberg. Incremental dynamic analysis applied to seismic financial risk assessment of bridges. *Engineering structures*, 29(10):2662–2672, 2007.

[8] NA Abrahamson. Seismic hazard assessment: problems with current practice and future developments. In *First European conference on earthquake engineering and seismology*, pages 3–8, 2006.

[9] Nicolas Luco and Paolo Bazzurro. Does amplitude scaling of ground motion records result in biased nonlinear structural drift responses? *Earthquake Engineering & Structural Dynamics*, 36(13):1813–1835, 2007.

[10] Peter J Stafford and Julian J Bommer. Theoretical consistency of common record selection strategies in performance-based earthquake engineering. In *Advances in Performance-Based Earthquake Engineering*, pages 49–58. Springer, 2010.

[11] Yin-Nan Huang, Andrew S Whittaker, Nicolas Luco, and Ronald O Hamburger. Scaling earthquake ground motions for performance-based assessment of buildings. *Journal of Structural Engineering*, 137(3):311–321, 2009.

[12] Iunio Iervolino, Flavia De Luca, and Edoardo Cosenza. Spectral shape-based assessment of SDOF nonlinear response to real, adjusted and artificial accelerograms. *Engineering Structures*, 32(9):2776–2792, 2010.

[13] AE Seifried and JW Baker. Spectral variability and its relationship to structural response estimated from scaled and spectrum-matched ground motions. *Earthquake Spectra*, 32(4):2191–2205, 2016.

[14] Laura Eads, Eduardo Miranda, and Dimitrios G Lignos. Average spectral acceleration as an intensity measure for collapse risk assessment. *Earthquake Engineering & Structural Dynamics*, 44(12):2057–2073, 2015.

[15] Mohsen Kohrangi, Sreeram Reddy Kotha, and Paolo Bazzurro. Ground-motion models for average spectral acceleration in a period range: direct and indirect methods. *Bulletin of Earthquake Engineering*, 16(1):45–65, 2018.

[16] P Bazzurro and CA Cornell. Vector-valued probabilistic seismic hazard analysis (VPSHA). In *Proceedings of the 7th US national conference on earthquake engineering*, pages 21–25, 2002.

[17] Jack W Baker and C Allin Cornell. A vector-valued ground motion intensity measure consisting of spectral acceleration and epsilon. *Earthquake Engineering & Structural Dynamics*, 34(10):1193–1217, 2005.

[18] Jack W Baker. Probabilistic structural response assessment using vector-valued intensity measures. *Earthquake Engineering & Structural Dynamics*, 36(13):1861–1883, 2007.

[19] Mohsen Kohrangi, Paolo Bazzurro, and Dimitrios Vamvatsikos. Vector and scalar IMs in structural response estimation, part I: Hazard analysis. *Earthquake Spectra*, 32(3):1507–1524, 2016.

[20] Mohsen Kohrangi, Paolo Bazzurro, and Dimitrios Vamvatsikos. Vector and scalar IMs in structural response estimation, part II: building demand assessment. *Earthquake Spectra*, 32(3):1525–1543, 2016.

[21] Jack W Baker and C Allin Cornell. Spectral shape, epsilon and record selection. *Earthquake Engineering & Structural Dynamics*, 35(9):1077–1095, 2006.

[22] Brendon A Bradley. A generalized conditional intensity measure approach and holistic ground-motion selection. *Earthquake Engineering & Structural Dynamics*, 39(12):1321–1342, 2010.

[23] Mohsen Kohrangi, Paolo Bazzurro, Dimitrios Vamvatsikos, and Andrea Spillatura. Conditional spectrum-based ground motion record selection

using average spectral acceleration. *Earthquake Engineering & Structural Dynamics*, 46(10):1667–1685, 2017.

[24] Carlos A Arteta and Norman A Abrahamson. Conditional scenario spectra (CSS) for hazard-consistent analysis of engineering systems. *Earthquake Spectra*, 35(2):737–757, 2019.

[25] Mohsen Kohrangi, Dimitrios Vamvatsikos, and Paolo Bazzurro. Multi-level conditional spectrum-based record selection for ida. *Earthquake Spectra*, 36(4):1976–1994, 2020.

[26] Andrea Spillatura, Mohsen Kohrangi, Paolo Bazzurro, and Dimitrios Vamvatsikos. Conditional spectrum record selection faithful to causative earthquake parameter distributions. *Earthquake Engineering & Structural Dynamics*, 2021.

[27] Dimitrios Vamvatsikos and C. Allin Cornell. Incremental dynamic analysis. *Earthquake Engineering & Structural Dynamics*, 31(3):491–514, 2002.

[28] Jeongeun Son and Yuncheng Du. Comparison of intrusive and nonintrusive polynomial chaos expansion-based approaches for high dimensional parametric uncertainty quantification and propagation. *Computers & Chemical Engineering*, 134:106685, 2020.

[29] Dimitrios Vamvatsikos. Seismic performance uncertainty estimation via ida with progressive accelerogram-wise latin hypercube sampling. *Journal of Structural Engineering*, 140(8):A4014015, 2014.

[30] Beliz U Gokkaya, Jack W Baker, and Greg G Deierlein. Quantifying the impacts of modeling uncertainties on the seismic drift demands and col-

lapse risk of buildings with implications on seismic design checks. *Earthquake Engineering & Structural Dynamics*, 45(10):1661–1683, 2016.

[31] Jun Xu, Wangxi Zhang, and Rui Sun. Efficient reliability assessment of structural dynamic systems with unequal weighted quasi-monte carlo simulation. *Computers & Structures*, 175:37–51, 2016.

[32] Denny Thaler, Marcus Stoffel, Bernd Markert, and Franz Bamer. Machine-learning-enhanced tail end prediction of structural response statistics in earthquake engineering. *Earthquake Engineering & Structural Dynamics*, 50(8):2098–2114, 2021.

[33] Paolo Bazzurro, C Allin Cornell, Nilesh Shome, and Jorge E Carballo. Three proposals for characterizing MDOF nonlinear seismic response. *Journal of Structural Engineering*, 124(11):1281–1289, 1998.

[34] Hexiang Wang, Fangbo Wang, Han Yang, Yuan Feng, Jeff Bayless, Norman A. Abrahamson, and Boris Jeremić. Time domain intrusive probabilistic seismic risk analysis of nonlinear shear frame structure. *Soil Dynamics and Earthquake Engineering*, 136:106201, 2020. ISSN 0267-7261. doi: https://doi.org/10.1016/j.soildyn.2020.106201. URL http://www.sciencedirect.com/science/article/pii/S0267726119313016.

[35] Konstantinos Karapiperis, Kallol Sett, M. Levent Kavvas, and Boris Jeremić. Fokker-planck linearization for non-gaussian stochastic elastoplastic finite elements. *Computer Methods in Applied Mechanics and Engineering*, 307:451–469, 2016.

[36] James N Brune. Tectonic stress and the spectra of seismic shear waves from earthquakes. *Journal of geophysical research*, 75(26):4997–5009, 1970.

[37] David M Boore. Stochastic simulation of high-frequency ground motions based on seismological models of the radiated spectra. *Bulletin of the Seismological Society of America*, 73(6A):1865–1894, 1983.

[38] David M. Boore. Simulation of ground motion using the stochastic method. *Pure and Applied Geophysics*, 160:635–676, 2003.

[39] David M Boore and Eric M Thompson. Revisions to some parameters used in stochastic-method simulations of ground motion. *Bulletin of the Seismological Society of America*, 105(2A):1029–1041, 2015.

[40] David M Boore. *SMSIM: Fortran programs for simulating ground motions from earthquakes: Version 2.3*. Citeseer, 2005.

[41] Roger G. Ghanem and Pol D. Spanos. *Stochastic Finite Elements, A Spectral Approach*. Dover Publications Inc., revised edition edition, 1991.

[42] Kallol Sett, Boris Jeremić, and M. Levent Kavvas. Stochastic elastic-plastic finite elements. *Computer Methods in Applied Mechanics and Engineering*, 200(9-12):997–1007, February 2011. ISSN 0045-7825. doi: DOI:10.1016/j.cma.2010.11.021.

[43] Sanjay Singh Bora, Frank Scherbaum, Nicolas Kuehn, and Peter Stafford. On the relationship between fourier and response spectra: Implications for the adjustment of empirical ground-motion prediction equations (GMPEs). *Bulletin of the Seismological Society of America*, 106(3):1235–1253, 2016.

[44] Sanjay Singh Bora, Frank Scherbaum, Nicolas Kuehn, Peter Stafford, and Benjamin Edwards. Development of a response spectral ground-motion prediction equation (GMPE) for seismic-hazard analysis from

empirical fourier spectral and duration models. *Bulletin of the Seismological Society of America*, 105(4):2192–2218, 2015.

[45] Sanjay Singh Bora, Fabrice Cotton, and Frank Scherbaum. NGA-West2 empirical fourier and duration models to generate adjustable response spectra. *Earthquake Spectra*, page 2, 2018.

[46] Jeff Bayless and Norman A Abrahamson. Evaluation of the interperiod correlation of ground-motion simulations. *Bulletin of the Seismological Society of America*, 108(6):3413–3430, 2018.

[47] Jeff Bayless and Norman A Abrahamson. Summary of the ba18 ground-motion model for fourier amplitude spectra for crustal earthquakes in california. *Bulletin of the Seismological Society of America*, 109(5):2088–2105, 2019.

[48] Jeff Bayless and Norman A Abrahamson. An empirical model for the interfrequency correlation of epsilon for fourier amplitude spectra. *Bulletin of the Seismological Society of America*, 109(3):1058–1070, 2019.

[49] Norman A Abrahamson. What changes to expect in seismic hazard analyses in the next 5 years, 2018. Plenary talk at the 11th U.S. National Conference on Earthquake Engineering, Los Angeles, United States.

[50] Hjörtur Thráinsson and Anne S Kiremidjian. Simulation of digital earthquake accelerograms using the inverse discrete fourier transform. *Earthquake engineering & structural dynamics*, 31(12):2023–2048, 2002.

[51] V Montaldo, AS Kiremidjian, H Thrainsson, and G Zonno. Simulation of the fourier phase spectrum for the generation of synthetic accelerograms. *Journal of Earthquake Engineering*, 7(03):427–445, 2003.

[52] David M Boore. Phase derivatives and simulation of strong ground motions. *Bulletin of the Seismological Society of America*, 93(3):1132–1143, 2003.

[53] Tadanobu Sato. Fractal characteristics of phase spectrum of earthquake motion. *Journal of Earthquake and Tsunami*, 7(02):1350010, 2013.

[54] Marco Gaetano Baglio. *Stochastic ground motion method combining a Fourier amplitude spectrum model from a response spectrum with application of phase derivatives distribution prediction*. PhD thesis, Politecnico di Torino, 2017.

[55] Robin K McGuire. *Seismic hazard and risk analysis*. Earthquake Engineering Research Institute, 2004.

[56] Edward H Field, Thomas H Jordan, and C Allin Cornell. OpenSHA: A developing community-modeling environment for seismic hazard analysis. *Seismological Research Letters*, 74(4):406–419, 2003.

[57] Christie Hale, Norman Abrahamson, and Yousef Bozorgnia. Probabilistic seismic hazard analysis code verification. Technical Report PEER 2018/03, Pacific Earthquake Engineering Research Center, Headquarters at the University of California, Berkeley, 2018.

[58] Edward H. Field, Thomas H. Jordan, Morgan T. Page, Kevin R. Milner, Bruce E. Shaw, Timothy E. Dawson, Glenn P. Biasi, Tom Parsons, Jeanne L. Hardebeck, Andrew J. Michael, II Ray J. Weldon, Peter M. Powers, Kaj M. Johnson, Yuehua Zeng, Karen R. Felzer, Nicholas van der Elst, Christopher Madden, Ramon Arrowsmith, Maximilian J. Werner, and Wayne R. Thatcher. A synoptic view of the third Uniform

California Earthquake Rupture Forecast (UCERF3). *Seismological Research Letters*, 88(5):1259–1267, 2017.

[59] Peter J Stafford. Interfrequency correlations among fourier spectral ordinates and implications for stochastic ground-motion simulationinterfrequency correlations among fourier spectral ordinates and implications. *Bulletin of the Seismological Society of America*, 107(6):2774–2791, 2017.

[60] Roger Musson. On the nature of logic trees in probabilistic seismic hazard assessment. *Earthquake Spectra*, 28(3):1291–1296, 2012.

[61] Y Ohsaki. On the significance of phase content in earthquake ground motions. *Earthquake Engineering & Structural Dynamics*, 7(5):427–439, 1979.

[62] Fangbo Wang and Kallol Sett. Time-domain stochastic finite element simulation of uncertain seismic wave propagation through uncertain heterogeneous solids. *Soil Dynamics and Earthquake Engineering*, 88: 369 – 385, 2016. ISSN 0267-7261. doi: http://dx.doi.org/10.1016/j.soildyn.2016.07.011. URL http://www.sciencedirect.com/science/article/pii/S0267726116300896.

[63] S. Sakamoto and R. Ghanem. Polynomial chaos decomposition for the simulation of non-gaussian nonstationary stochastic processes. *Journal of Engineering Mechanics*, 128(2):190–201, February 2002.

[64] Zhibao Zheng and Hongzhe Dai. Simulation of multi-dimensional random fields by Karhunen-Loève expansion. *Computer Methods in Applied Mechanics and Engineering*, 324:221 – 247, 2017. doi: http://dx.

doi.org/10.1016/j.cma.2017.05.022. URL http://www.sciencedirect.com/science/article/pii/S0045782516318692.

[65] K.K. Phoon, H.W. Huang, and S.T. Quek. Simulation of strongly non-gaussian process using Karhunen-Loève expansion. *Probabilistic Engineering Mechanics*, 20:188–198, June 2005.

[66] Boris Jeremić, Zhaohui Yang, Zhao Cheng, Guanzhou Jie, Nima Tafazzoli, Matthias Preisig, Panagiota Tasiopoulou, Federico Pisanò, José Abell, Kohei Watanabe, Yuan Feng, Sumeet Kumar Sinha, Fatemah Behbehani, Han Yang, and Hexiang Wang. *Nonlinear Finite Elements: Modeling and Simulation of Earthquakes, Soils, Structures and their Interaction*. University of California, Davis, CA, USA, 1989-2021. ISBN 978-0-692-19875-9. URL: http://sokocalo.engr.ucdavis.edu/~jeremic/LectureNotes/.

[67] Manas K Deb, Ivo M Babuška, and J Tinsley Oden. Solution of stochastic partial differential equations using galerkin finite element techniques. *Computer Methods in Applied Mechanics and Engineering*, 190(48): 6359–6372, 2001.

[68] Nathan. M. Newmark. A method of computation for structural dynamics. *ASCE Journal of the Engineering Mechanics Division*, 85:67–94, July 1959.

[69] Hermann G. Matthies and Andreas Keese. Galerkin methods for linear and nonlinear elliptic stochastic partial differential equations. *Computational Methods in Applied Mechanics and Engineering*, 194(1):1295–1331, April 2005.

[70] M. Arnst and R. Ghanem. A variational-inequality approach to stochastic boundary value problems with inequality constraints and its application to contact and elastoplasticity. *International Journal for Numerical Methods in Engineering*, 89(13):1665–1690, 2012. ISSN 1097-0207. doi: 10.1002/nme.3307. URL http://dx.doi.org/10.1002/nme.3307.

[71] Bruno Sudret. Global sensitivity analysis using polynomial chaos expansions. *Reliability Engineering & System Safety*, 93(7):964 – 979, 2008. ISSN 0951-8320. doi: https://doi.org/10.1016/j.ress.2007.04.002. URL http://www.sciencedirect.com/science/article/pii/S0951832007001329. Bayesian Networks in Dependability.

[72] Dongbin Xiu and J. S. Hesthaven. High-order collocation methods for differential equations with random inputs. *SIAM Journal on Scientific Computing*, 27(3):1118–1139, 2005.

[73] Patricia Thomas, Ivon Wong, Judith Zachariasen, Robert Darragh, and Walt Silva. 2013 update to the site-specific seismic hazard analysis and development of seismic design ground motions. Technical report, URS Corporation, Oakland, CA, 2014.

[74] Robert R Youngs and Kevin J Coppersmith. Implications of fault slip rates and earthquake recurrence models to probabilistic seismic hazard estimates. *Bulletin of the Seismological society of America*, 75(4):939–964, 1985.

[75] FEMA-365. Prestandard and commentary for the seismic rehabilitation of buildings. Technical report, Federal Emergency Management Agency, Washington DC., 2000.

[76] Derya Deniz, Junho Song, and Jerome F Hajjar. Energy-based seismic collapse criterion for ductile planar structural frames. *Engineering Structures*, 141:1–13, 2017.

[77] Derya Deniz, Junho Song, and Jerome F Hajjar. Energy-based sidesway collapse fragilities for ductile structural frames under earthquake loadings. *Engineering Structures*, 174:282–294, 2018.

[78] Alexios Papasotiriou, Asimina Athanatopoulou, and Konstantinos Kostinakis. Investigation on engineering demand parameters describing the seismic damage of masonry infilled R/C frames. *Bulletin of Earthquake Engineering*, 18(13):6075–6115, 2020.

[79] Gail M Atkinson and Walt Silva. An empirical study of earthquake source spectra for california earthquakes. *Bulletin of the Seismological Society of America*, 87(1):97–113, 1997.

[80] Annemarie S Baltay, Thomas C Hanks, and Norm A Abrahamson. Uncertainty, variability, and earthquake physics in ground-motion prediction equations. *Bulletin of the Seismological Society of America*, 107(4): 1754–1772, 2017.

[81] Boris Jeremić, Guanzhou Jie, Zhao Cheng, Nima Tafazzoli, Panagiota Tasiopoulou, Federico Pisanò, José Antonio Abell, Kohei Watanabe, Yuan Feng, Sumeet Kumar Sinha, Fatemah Behbehani, Han Yang, and Hexiang Wang. *The Real-ESSI Simulator System*. University of California, Davis, 1988-2021. http://real-essi.us/.